Acta Biomaterialia 29 (2016) 409–423

Contents lists available at ScienceDirect

Acta Biomaterialia

journal homepage: www.elsevier.com/locate/actabiomat

Guided bone regeneration using resorbable membrane and different bone substitutes: Early histological and molecular events

Ibrahim Elgali [a,b,1], Alberto Turri [a,b,c,1], Wei Xia [e], Birgitta Norlindh [a,b], Anna Johansson [a,b], Christer Dahlin [a,b,d], Peter Thomsen [a,b,*], Omar Omar [a,b]

[a] BIOMATCELL VINN Excellence Center of Biomaterials and Cell Therapy, Gothenburg, Sweden
[b] Department of Biomaterials, Institute of Clinical Sciences, Sahlgrenska Academy, University of Gothenburg, Box 412, SE-405 30 Gothenburg, Sweden
[c] The Brånemark Clinic, Institute of Odontology, Public Dental Health Care, Gothenburg, Sweden
[d] Department of Oral, Maxillofacial Surgery and Research and Development, NU-Hospital Organization, Trollhättan, Sweden
[e] Applied Material Sciences, Department of Engineering Sciences, Uppsala University, Box 534, 751 21 Uppsala, Sweden

ARTICLE INFO

Article history:
Received 10 June 2015
Received in revised form 3 September 2015
Accepted 2 October 2015
Available online 13 October 2015

Keywords:
Guided bone regeneration
Membrane
Bone substitute
Strontium
Gene expression

ABSTRACT

Bone insufficiency remains a major challenge for bone-anchored implants. The combination of guided bone regeneration (GBR) and bone augmentation is an established procedure to restore the bone. However, a proper understanding of the interactions between the bone substitute and GBR membrane materials and the bone-healing environment is lacking. This study aimed to investigate the early events of bone healing and the cellular activities in response to a combination of GBR membrane and different calcium phosphate (CaP) materials. Defects were created in the trabecular region of rat femurs, and filled with deproteinized bovine bone (DBB), hydroxyapatite (HA) or strontium-doped HA (SrHA) or left empty (sham). All the defects were covered with an extracellular matrix membrane. Defects were harvested after 12 h, 3 d and 6 d for histology/histomorphometry, immunohistochemistry and gene expression analyses. Histology revealed new bone, at 6 d, in all the defects. Larger amount of bone was observed in the SrHA-filled defect. This was in parallel with the reduced expression of osteoclastic genes (CR and CatK) and the osteoblast–osteoclast coupling gene (RANKL) in the SrHA defects. Immunohistochemistry indicated fewer osteoclasts in the SrHA defects. The observations of CD68 and periostin-expressing cells in the membrane *per se* indicated that the membrane may contribute to the healing process in the defect. It is concluded that the bone-promoting effects of Sr *in vivo* are mediated by a reduction in catabolic and osteoblast–osteoclast coupling processes. The combination of a bioactive membrane and CaP bone substitute material doped with Sr may produce early synergistic effects during GBR.

Statement of significance

The study provides novel molecular, cellular and structural evidence on the promotion of early bone regeneration in response to synthetic strontium-containing hydroxyapatite (SrHA) substitute, in combination with a resorbable, guided bone regeneration (GBR) membrane. The prevailing view, based mainly upon *in vitro* data, is that the beneficial effects of Sr are exerted by the stimulation of bone-forming cells (osteoblasts) and the inhibition of bone-resorbing cells (osteoclasts). In contrast, the present study demonstrates that the local effect of Sr *in vivo* is predominantly via the inhibition of osteoclast number and activity and the reduction of osteoblast–osteoclast coupling. This experimental data will form the basis for clinical studies, using this material as an interesting bone substitute for guided bone regeneration.

1. Introduction

The combination of bone substitute materials and membrane is commonly used to restore lost or defective bone under the original treatment concept of guided bone regeneration (GBR). While the membranes would isolate the bone defect site from

* Corresponding author at: Department of Biomaterials, Institute of Clinical Sciences, Sahlgrenska Academy, University of Gothenburg, Box 412, SE-405 30 Gothenburg, Sweden.
E-mail address: peter.thomsen@biomaterials.gu.se (P. Thomsen).
[1] Equal contribution.

http://dx.doi.org/10.1016/j.actbio.2015.10.005
1742-7061/

non-osteogenic soft tissue, the bone substitute would maintain a three-dimensional scaffold to support the osteogenic cells and tissue during bone healing. However, a hypothesis as such remains speculative, since the mechanisms of bone healing and regeneration, in conjunction with the membrane and bone substitutes, have not been sufficiently described.

Different types of biomaterials are used as bone substitutes and as membrane with variable outcomes. Optimizations, for the predictable outcomes of these biomaterials, require a proper understanding of the interactions between the substitute and membrane components with the local host environment. This includes the influence of the biomaterial properties on the early cellular and molecular events that determine the onset of tissue healing and may eventually affect the overall defect restitution.

Deproteinized bovine bone (DBB) is a natural hydroxyapatite and it is by far the best-documented xenogenic calcium-phosphate-based material used as a bone substitute. Clinical studies have reported that DBB promotes bone healing and implant osseointegration during GBR [1,2]. Nevertheless, other studies have shown that DBB fails to enhance bone formation or might even inhibit osseous healing [3,4]. Over the last few years, a substantial amount of research has been performed to improve the properties of synthetic calcium phosphate materials. Synthetic hydroxyapatite (HA) resembles the chemical composition of the inorganic component of bone. Nevertheless, the mineral phase of bone is not purely hydroxyapatite and contains traces of other elements. The roles of specific elements in bone formation and structure are not fully understood. It has therefore been suggested that the incorporation of specific inorganic ions into the scaffold CaP material might favorably affect bone regeneration [5]. One example of importance is strontium (Sr), which has demonstrated favorable effects on bone quality and strength when administered systemically. *In vitro* studies have suggested that Sr has the potential to increase osteoblastic cell proliferation, gene expression and functional activities [6,7], although the anabolic effect of Sr has been questioned [8]. Other *in vitro* studies have suggested that Sr interferes directly with osteoclasts and their resorptive activity [9,10]. Nevertheless, the role of Sr incorporation in HA material on the *in vivo* events of early inflammation, bone formation and remodeling needs to be determined.

A rationale to study the interactions between materials and cells during the early time periods is derived from observations *in vivo* which have shown that material properties are rapidly sensed by material-adherent cells [11]. These interactions modulate RANKL/OPG/RANK expression, osteoid formation, bone maturation, osseointegration and implant-bone stability.

The overall objective of this study was to determine the relationship between early bone regeneration in bone defects and cellular distribution and activities in association with different calcium phosphate materials under GBR membrane. The early molecular and cellular processes, potentially involved in GBR, were investigated in a rat femur model using a novel strontium-doped hydroxyapatite (SrHA) compared with hydroxyapatite (HA) and deproteinized bovine bone (DBB). The cellular and molecular activities were related to the overall early bone formation and to the spatial distribution of the newly formed bone. The aims were, firstly, to determine whether the presence of bone substitutes in membrane-covered defects alters the early bone formation, compared with empty, membrane-covered defects. Secondly, does the presence of Sr ions in the HA affect the early cellular and molecular activities in the defect and, if so, does this relate to the amount and distribution of the new bone? In addition, a third aim was to explore whether monocytes/macrophages and osteoprogenitors are distributed in the membrane *per se*.

2. Material and methods

2.1. Materials

Deproteinized bovine bone (DBB; Bio-Oss) was purchased from Geistlich Pharma AG (Wolhusen, Switzerland). For the in-house preparation of the hydroxyapatite (HA) and the strontium-doped hydroxyapatite (SrHA), calcium chloride, strontium nitrate, diammonium hydrogen phosphate and ammonia solution were purchased from Sigma–Aldrich (USA). All the chemicals were analytical grade reagents used as received without further purification.

2.1.1. Preparation of powders (HA, SrHA005, SrHA025 and SrHA050)

Firstly, HA powder was synthesized using a standardized precipitation method. In short, 0.2 M of diammonium hydrogen phosphate solution (S1) and 0.33 M of calcium nitrate solution (S2) were prepared separately. The Ca/P ratio and the pH value were adjusted to 1.67 and 10 respectively. The S1 was gradually added to S2 by stirring. The precipitation was kept for 24 h before filtration and washing. Finally, the precipitation was washed twice with distilled water and once with ethanol, before drying at 60 °C in a vacuum oven. The SrHA powder was prepared in the same way but also with the addition of strontium nitrate to the S2 solution. For characterization purposes, SrHA powders with three levels of Ca substitution by Sr were prepared: 5% (SrHA005), 25% (SrHA025) and 50% (SrHA050). This was achieved by controlling the ratios of the Ca and Sr in the solution.

2.1.2. Preparation of granules (HA, SrHA005, SrHA025 and SrHA050)

The prepared HA, SrHA005, SrHA025 and SrHA050 powders were made into paste by mixing them with 0.6 wt% cellulose solution. The obtained pastes were injected into pores of Teflon plate with a thickness of 1.5 mm. The injected pastes were dried at 37 °C for 1 d. The as-prepared column-shaped granules (1.5 mm diameter) were then carefully removed from the Teflon plate and heat-treated (calcinated) at 1000 °C for 1 h. The obtained granules were then pulverized and sieved, using meshes, in order to obtain smaller granules with a size comparable to that of the DBB (in the range of 400–600 μm).

2.1.3. Characterizations of the granules (DBB, HA, SrHA005, SrHA025 and SrHA050)

All granule types were characterized with respect to surface area, crystallinity, *in vitro* degradation and *in vitro* ion release. Details about the different procedures and results of the characterizations are provided in the Supplementary material (Appendix A) and Supplementary Fig. S1. The results of the characterization tests showed that SrHA050 granules had a high release of Sr but not Ca or P, while displaying a surface area and degradation rate comparable to that of the HA granules. SrHA050 was therefore selected from the three groups with different Sr concentrations and designated as SrHA in the further characterizations (surface morphology and chemical composition) and in the *in vivo* studies.

2.1.4. Surface morphology and chemical composition of granules (DBB, HA, SrHA)

The morphology of the granules was analyzed using a field-emission scanning electron microscope (FESEM, LEO 1550) working at 5 kV. The chemical composition of the different granules and the number of different ions in each granule type were analyzed by inductively coupled plasma atomic emission spectroscopy (ICP-AES). In short, the granules were dissolved in 1 M of HCl solution and analyzed by ICP-AES.

2.2. Experimental design and animal model

2.2.1. Pre-testing in polyurethane foam

The amount of each granule type (DBB, HA and SrHA) needed to fill a comparable defect size in the animal model was estimated by filling holes created in solid rigid polyurethane foams (Sawbones®, Pacific Research Laboratories, Vashon, USA). The holes were created in the polyurethane foam block using a trephine (2.3 mm diameter and 3 mm penetration depth). An optimum amount of each granule type was then incrementally added to the holes, ensuring complete filling. Thereafter, the weight of each granule type needed to fill the standardized defect size was measured. The mean weight of DBB, HA and SrHA was 1.1, 2.3 and 1.4 mg, respectively.

2.2.2. Animal surgery

The animal experiment was approved by the University of Gothenburg Local Ethics Committee for Laboratory Animals (dnr 279/2011). A total of 84 male Sprague–Dawley rats (Charles River, Sulzfeld, Germany) were used. The average weight ranged between 320 and 350 g. The handling of animals and the surgical protocol has previously been described in detail [11]. In brief, the surgical procedure was performed under inhalation general anesthesia and a local injection of xylocaine. A defect was made in each femoral epiphysis (trabecular bone region) using a trephine with a 2.3 mm internal diameter and 3 mm penetration depth under generous irrigation with NaCl 0.9%. Bone harvested from the defect site was collected from the trephine and preserved in RNA preservation medium for the determination of baseline gene expression (BL; $n = 8$). Each defect was filled with deproteinized bovine bone (DBB), hydroxyapatite (HA) or strontium-doped hydroxyapatite (SrHA) granules or left empty (sham). All defects, filled and empty, were then covered using an extracellular membrane derived from porcine small intestinal submucosa (DynaMatrix®, Keystone Dental, Burlington, MA, USA) (Fig. 1). The four experimental groups were randomized, ensuring equal distribution and rotation among the animals and between right and left locations. The retrieval procedure was performed at 12 h, 3 d and 6 d (28 rats at each time point). The skin was re-opened and the experimental sites were identified. Sites intended for gene expression analysis were retrieved using a 2.3 mm trephine. The samples were immediately preserved in tubes containing RNA*later* ($n = 8$ per group at each time point). Sites designated for histology and immunohistochemistry were harvested *en bloc* using a dental disc. The harvested samples were then immersed in formalin ($n = 6$ per group at each time point).

2.2.3. Histology and immunohistochemistry

After fixation, the blocks were decalcified in 10% EDTA for 10 d. Thereafter, the decalcified blocks were dehydrated twice in 70% ethanol and four times in iso-propylalcohol, for 1 h each. Subsequently, paraffin was infiltrated into the samples using liquid paraffin at 56–58 °C, 3 times for 1 h. After paraffin embedding, sections with a thickness of 3–5 μm were produced using a microtome, then mounted on glass slides and stained with hematoxylin and eosin for light microscopy.

For immunostaining, 3–5 μm paraffin-embedded sections were mounted on polylysine slides (Menzel GmbH and Co KG, Braunschweig, Germany). The sections were deparaffinized, hydrated and incubated with primary antibodies CD68 (sc-58965, Santa Cruz Biotechnology, USA) and periostin (ab14041, Abcam, UK). The CD68 targeted mononuclear cells (monocytes/macrophages), as well as multinucleated giant cells and osteoclasts. The periostin was used as a marker of osteoprogenitor cells and intramembranous bone formation [12]. Negative control slides were prepared by the omission of the primary antibody and incubation with 1% BSA in PBS. The immunoreactivity of CD68 and periostin was detected and visualized using Betazoid DAB Chromogen kit and horseradish peroxidase (HRP) (Biocare Medical, USA). The relative proportions of the CD68 positive cells were semi-quantitatively scored as three major subcategories: (i) mononuclear, monocyte/macrophage phenotypes, (ii) multinuclear, osteoclast phenotypes (associated with bone remodeling site) and (iii) multinuclear giant cell phenotypes (associated with material or in soft tissue). The counting procedure was applied (objective ×20). The number of cells/mm^2 was determined and the total amount was then calculated with respect to the total defect area. The periostin staining was evaluated qualitatively.

2.2.4. Histomorphometry

For histomorphometry, the paraffin-embedded blocks were re-embedded in acrylic resin (LR White) (London Resin Company Ltd, Berkshire, UK). The long axis of the defect was cut using a diamond saw. Ground sections were prepared using sawing and grinding (Exakt Apparatebau GmbH & Co, Norderstedt, Germany). Sections with a final thickness of 10–20 μm were stained with 1% toluidine blue. All sections were coded and evaluated blindly for histology and histomorphometry. Histomorphometry was performed using a 10× objective in a light microscope (Nikon Eclipse E600 Nikon Ltd., Tokyo, Japan) and image software (ACT-1; Nikon Ltd., Tokyo, Japan) and analytical software (Easy Image Measurement 2000; Bergman Labora AB, Huddinge, Sweden). The amount of newly formed bone in the defect was determined using a counting procedure. A software grid consisting of 16 zones (800 μm × 800 μm each) was superimposed over the tissue and the percentage area occupied by newly formed bone was calculated. In order to estimate the relative proportion and distribution of the bone in the defect, the following regions were identified: (I) the entire defect, represented by the 16 zones of the grid; (II) a peripheral region

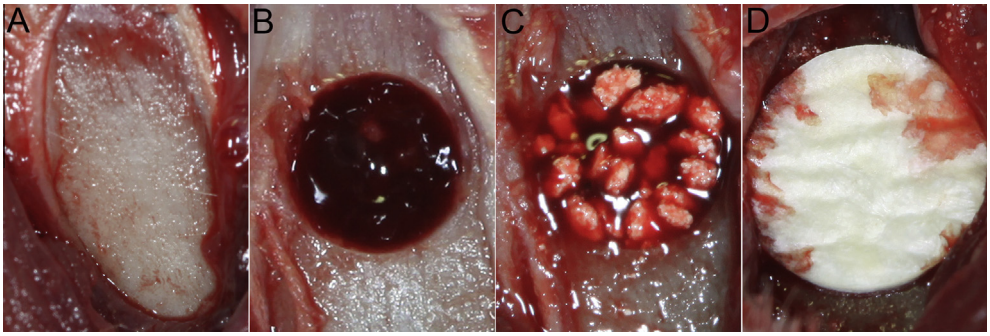

Fig. 1. The surgical procedure. The micrographs show the stepwise surgery: (A) site exposed; (B) defect prepared; (C) example of bone substitute (HA) introduced; (D) membrane applied.

(P, represented by zones covering the lateral and bottom borders of the defect) and a central region (C, represented by zones covering the center of the defect); (III) a top region (top, represented by the upper zones adjacent to the membrane), followed by a middle level (middle) and bottom level (bottom). The bone area was determined separately in every zone and the area percentage was then calculated with respect to the total defect area or to the respective region (central, peripheral, top, middle, bottom).

2.2.5. Quantitative polymerase chain reaction (qPCR)

Total RNA from the trephine-retrieved samples was extracted using an RNeasy Mini kit (QIAGEN GmbH, Hilden, Germany) according to previously published detailed procedure [11]. Reverse transcription was carried out using a GrandScript cDNA Synthesis kit (TATAA Biocenter AB, Gothenburg, Sweden) and universal RNA Spike (TATAA, Biocenter AB). The RNA concentration of each sample was normalized to 20 ng/ml before the reverse transcription. The design of primers for nine target genes, tumor necrosis factor-α (TNF-α), interleukin-6 (IL-6), monocyte chemoattractant protein-1 (MCP-1), chemokine receptor type 4 (CXCR-4), alkaline phosphatase (ALP), osteocalcin (OC), receptor activator of NF-kappaB ligand (RANKL), calcitonin receptor (CR) and cathepsin K (CatK), as well as for five putative reference genes, was performed using Primer3 software. Reference gene screening was performed on ten bone samples (two of each type) from each time point. The RNA quality of these samples was analyzed with a Nano 6000 RNA kit by Bioanalyser 2100 Electrophoresis System (Agilent Technologies). The expression profiles of the putative reference genes were evaluated using geNorm and Normfinder software (GenEx ver.6, Multid Analyses AB, Gothenburg, Sweden), in order to determine the best reference gene for normalization. The primer design parameters were in accordance with previously described procedure [11]. Real-time PCR was performed in duplicate using the CFX 96 Real time System (BIO RAD laboratories) with Grandmaster SYBR mix (TATAA Biocenter, Sweden) in 10 µl reactions. The cycling conditions were 95 °C for 30 s, followed by 40 cycles of 95 °C for 5 s, 60 °C for 15 s and 72 °C for 10 s. The fluorescence was read at the end of the 72 °C step. Melting curves were recorded after the run by a stepwise temperature increase (1 °C/5 s) from 65 to 95 °C. All plates were run with an Interplate calibrator (TATAA Biocenter, Sweden) to compensate for variations between runs. Both geNorm and Normfinder identified the gene hypoxanthine phosphoribosyltransferase 1 (HPRT1) as the most stable in the present experimental study. Quantities of the target genes were normalized to HPRT1. The normalized relative quantities were calculated using the delta-delta Cq method and 90% PCR efficiency ($k * 1.9^{\Delta\Delta Cq}$).

2.3. Statistical analysis

For histomorphometry and gene expression analyses, statistical comparisons were made between the four groups and between the different time points for each group. Moreover, the gene expression in the four groups was compared with the constitutive (baseline; BL) gene expression. A non-parametric Kruskal–Wallis test was used to identify statistical differences between the experimental groups or the time points. Whenever a statistical difference was found, the Mann–Whitney test was applied. Analyses were made using SPSS Version 10 software (SPSS, Inc., Chicago, USA) and the significance was set at $p < 0.05$. The data are presented as the mean ± standard error of the mean.

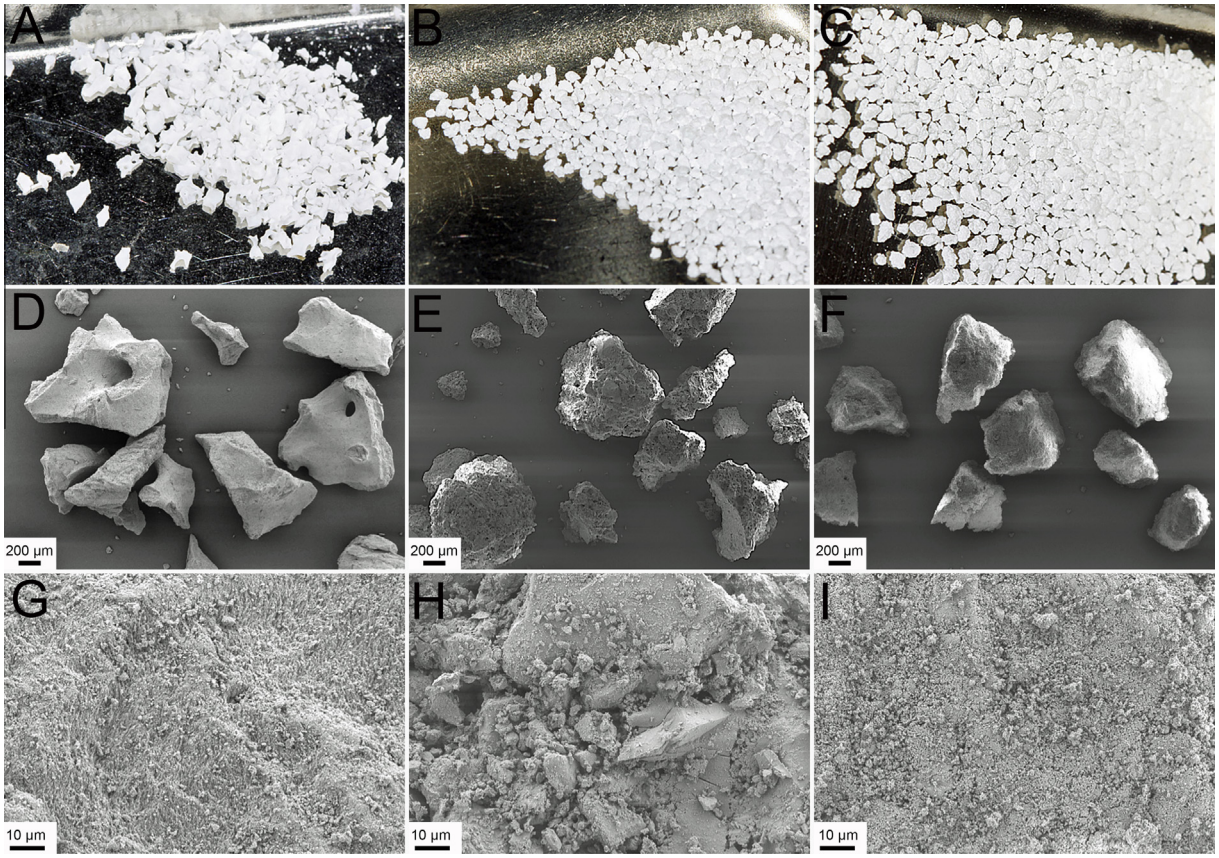

Fig. 2. Morphological evaluation of the substitute materials. The photographs (A–C) and scanning electron microscopy images (D–I) show the morphology of the different granules used to augment the bone defects. (A, D and G) show the deproteinized bovine bone (DBB); (B, E and H) show the hydroxyapatite (HA); (C, F and I) show the strontium-doped hydroxyapatite (SrHA).

3. Results

3.1. Surface morphology and composition of the different granules

Macroscopically, the DBB, HA and SrHA had a relatively similar appearance in terms of size range and surface irregularity (Fig. 2A–C). The SEM analysis at lower magnification showed that the individual DBB granules (Fig. 2D) had a greater variation in shape but presented a smoother surface than the HA and SrHA (Fig. 2E and F). No major difference between the HA and SrHA was observed at this magnification level. At higher magnification, whereas DBB (Fig. 2G) and SrHA (Fig. 2I) revealed a homogenously granular surface appearance, the HA (Fig. 2H) showed a combination of large and small grains. At this magnification, the DBB showed a smoother texture/curvature of the surface, whereas both the HA and SrHA displayed relatively sharp, needle-like structures. The data describing the elemental compositions of each granule type (DBB, HA and SrHA) are shown in Table 1.

Table 1
Chemical compositions of deproteinized bovine bone (DBB), hydroxyapatite (HA) and strontium-doped hydroxyapatite (SrHA) granules analyzed by inductively coupled plasma atomic emission spectroscopy (ICP-AES).

Material	Ca (mg/g)	Mg (mg/g)	P (mg/g)	Si (mg/g)	Sr (mg/g)
DBB	371	6.5	176	3	0.3
HA	364	0.2	190	0.09	44
SrHA	275	0.2	178	0.09	207

3.2. Histology and immunohistochemistry

At 12 h, the sham defect was mainly occupied by hematoma, whereas the augmented defects were occupied by evenly distributed bone substitutes (DBB, HA or SrHA). All substitutes were surrounded by hematoma consisting mainly of erythrocytes and a few strands of fibrin. Immunostaining at this time point revealed mononuclear, CD68-positive, monocytes/macrophages (Fig. 4), as well as periostin-positive osteoprogenitors, exhibiting a rounded shape (Fig. 5). No major differences in the relative proportion of the monocytes/macrophages (Table 2) or the osteoprogenitors were observed between the different experimental groups (sham, DBB, HA and SrHA).

At 3 d, the sham defect was occupied by a more organized hematoma, characterized by erythrocytes trapped in a dense fibrinous network (Fig. 3). In all bone substitute groups, the granules occupied a large portion of the defect and were confined within the boundaries of the defect (Fig. 3). The immunostaining showed that the relative proportion of CD68-positive monocytes/macrophages had increased considerably in all groups (Fig. 4). Scoring of these cells revealed that the higher increase was general in all substitute groups and to a lesser extent in the sham (Table 2). At this time point, periostin immunostained cells assumed more elongated, spindle-shaped morphology (Fig. 5). Moreover, diffuse staining of periostin was evident, predominantly at the surfaces of bone trabeculae bordering the defects. Diffuse staining of periostin was also detected interstitially in the intergranular tissues (Fig. 5). This diffuse staining of periostin, at 3 d, strongly indicated the earliest signs of intramembranous bone formation, which was not detected in the hematoxylin- and eosin-stained or toluidine blue-stained sections.

The HA group, at 6 d, was excluded from all immunohistochemical analyses due to poor quality sections for the cellular evaluations or counts. For the other groups (sham, DBB and SrHA) at 6 d, the hematoma observed in earlier time periods had been replaced by a well-organized granulation tissue rich in spindle-shaped cells (Figs. 3 and 5). In spite of this, the hematoma could still be observed in the central region of the sham defect (Fig. 3). The diffuse staining of periostin indicated a further increase in the amount and intensity, at the expense of the individually stained cells (Fig. 5). In parallel with the increased diffuse staining of periostin, new (woven) bone formation was observed in the sham defect and also in conjunction with all materials (DBB and SrHA) as judged using regular histology at 6 d (Fig. 6). The new, woven bone was preferentially localized at the periphery rather than in the center of the defects (Fig. 6). The SrHA group displayed

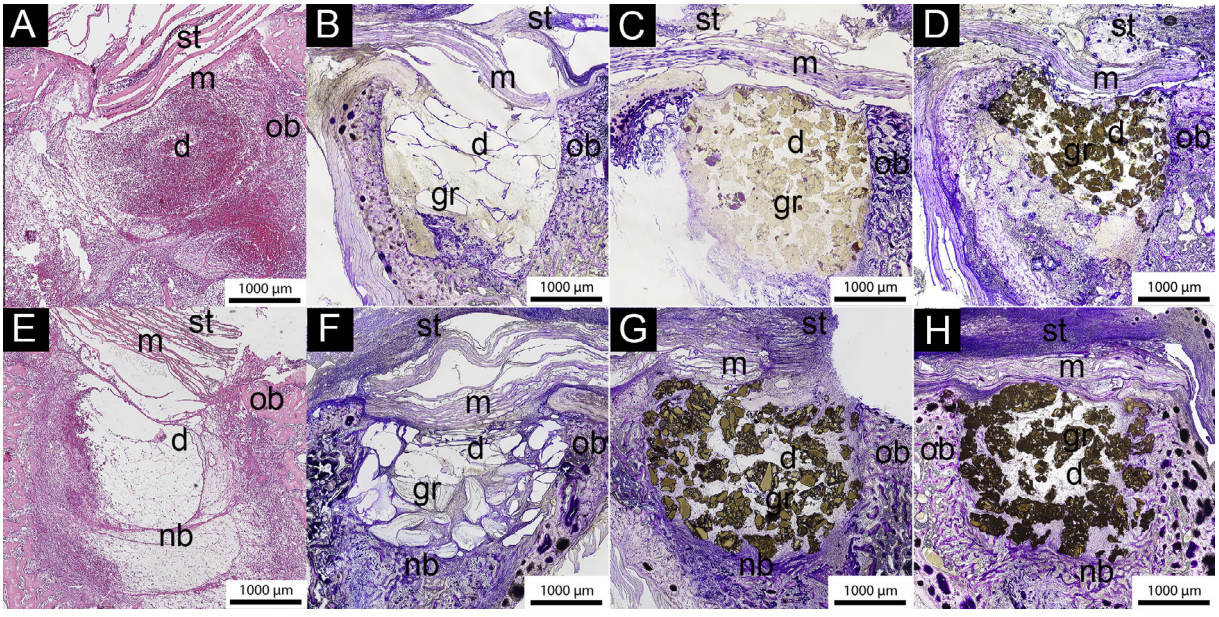

Fig. 3. Histology of the defects treated with membrane alone or membrane in combination with the different bone substitute materials. The survey micrographs show the four bone defect groups at 3 days (A–D) and 6 days (E–H) of implantation. The defects were either empty (sham; A and E) or filled with deproteinized bovine bone granules (DBB; B and F), hydroxyapatite granules (HA; C and G) or strontium-doped hydroxyapatite granules (SrHA; D and H). St = soft tissue; m = membrane; gr = granule; d = defect; ob = old bone; nb = new bone.

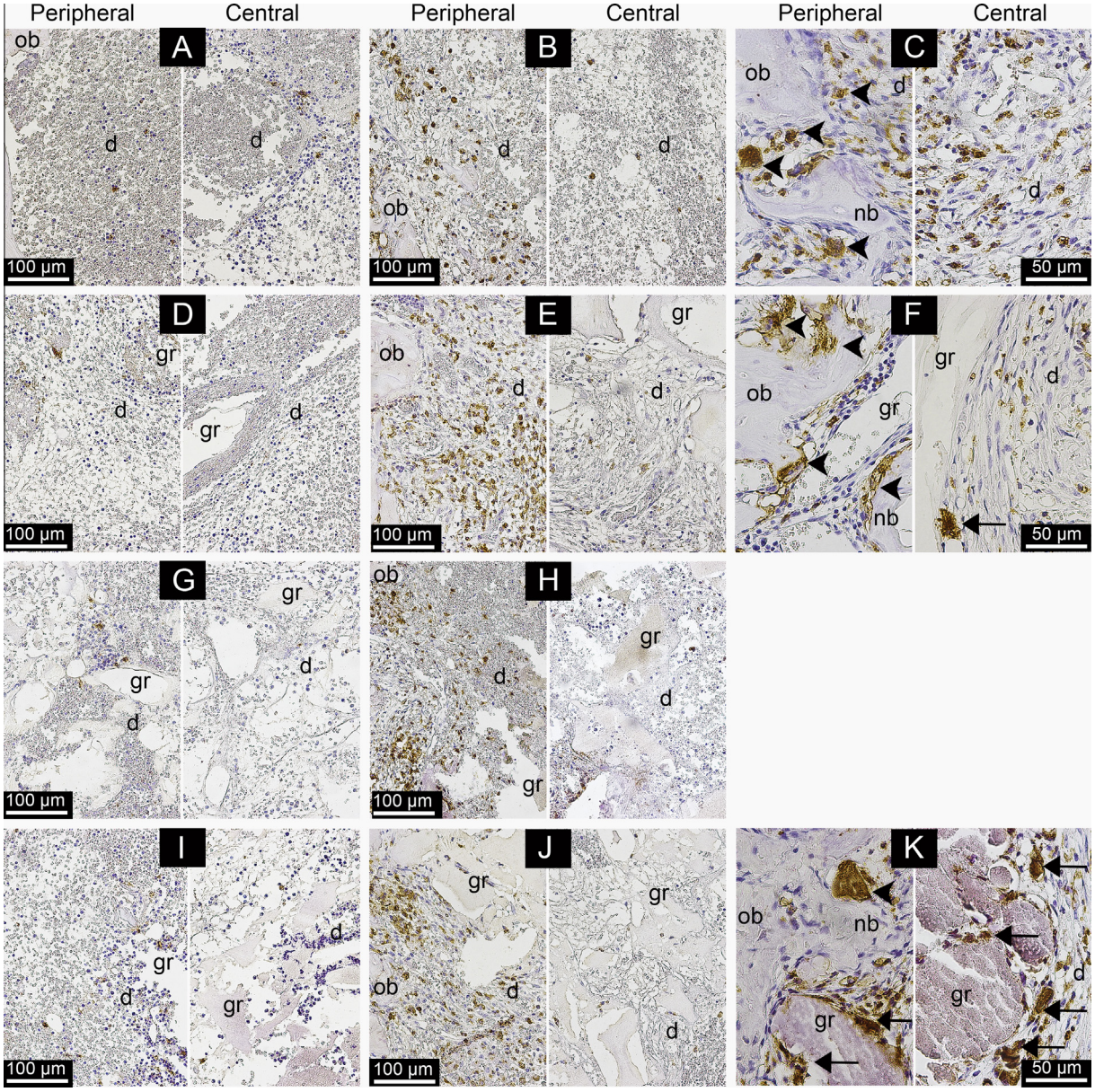

Fig. 4. Immunohistochemical analysis of CD68 reactivity in the defects treated with membrane alone or membrane in combination with the different bone substitute materials. The survey micrographs show selected central and peripheral regions of the defects treated with the membrane alone (sham; A–C) or the membrane in combination with deproteinized bovine bone granules (DBB; D–F), hydroxyapatite granules (HA; G and H) or strontium-doped hydroxyapatite granules (SrHA; I-K). The analysis was performed at 12 h (A, D, G and I), 3 days (B, E, H and J) and 6 days (C, F and K) of implantation. The membrane with hydroxyapatite granules (HA) group at 6 days was excluded from this analysis due to technical limitations in obtaining proper paraffin-embedded sections. Black arrowheads = bone-related multinucleated cells (osteoclasts); Black arrows = material-related multinucleated cells; ob = old bone; nb = new bone; d = defect; gr = granule.

more bone in the peripheral region compared with the equivalent regions in the other defects. Moreover, in the sham defects, the woven bone was restricted to the original bone at the periphery of the defect and was seldom detected centrally. In contrast, for all bone substitutes, islets of woven bone were also detected in the central region of the defect, lining the circumference of the granules. The border between the new bone and the DBB granules was clearly distinguishable. In contrast, in the case of the SrHA, the boundary was less easily distinguished and the woven bone occasionally appeared to reach into the surface irregularities of the granules.

With respect to CD68 immunostaining at 6 d (Fig. 4), it was noteworthy that an increase in the CD68-stained mononuclear monocytes/macrophages was observed in the sham defects. This resulted in the almost doubling of these cells in the sham compared with 3 d (Table 2). An important, exclusive observation at the 6 d time point was the appearance of many CD68-positive multinucleated cells within the boundaries of the different defects (Fig. 4). These multinucleated cells were seen repeatedly in two different relationships. The first was their close association with apparently active bone remodeling sites, characterized by resorption lacunae in the bone underneath these cells and osteoblastic seams depositing new bone (Fig. 4). The second was the appearance in association with substitute materials (SrHA and DBB) or scattered in the intergranular tissue between the granules of these materials (Fig. 4). The former were considered to be active osteoclasts, whereas the latter were referred to as multinucleated giant cells (MNGCs). The material-related MNGCs were more commonly

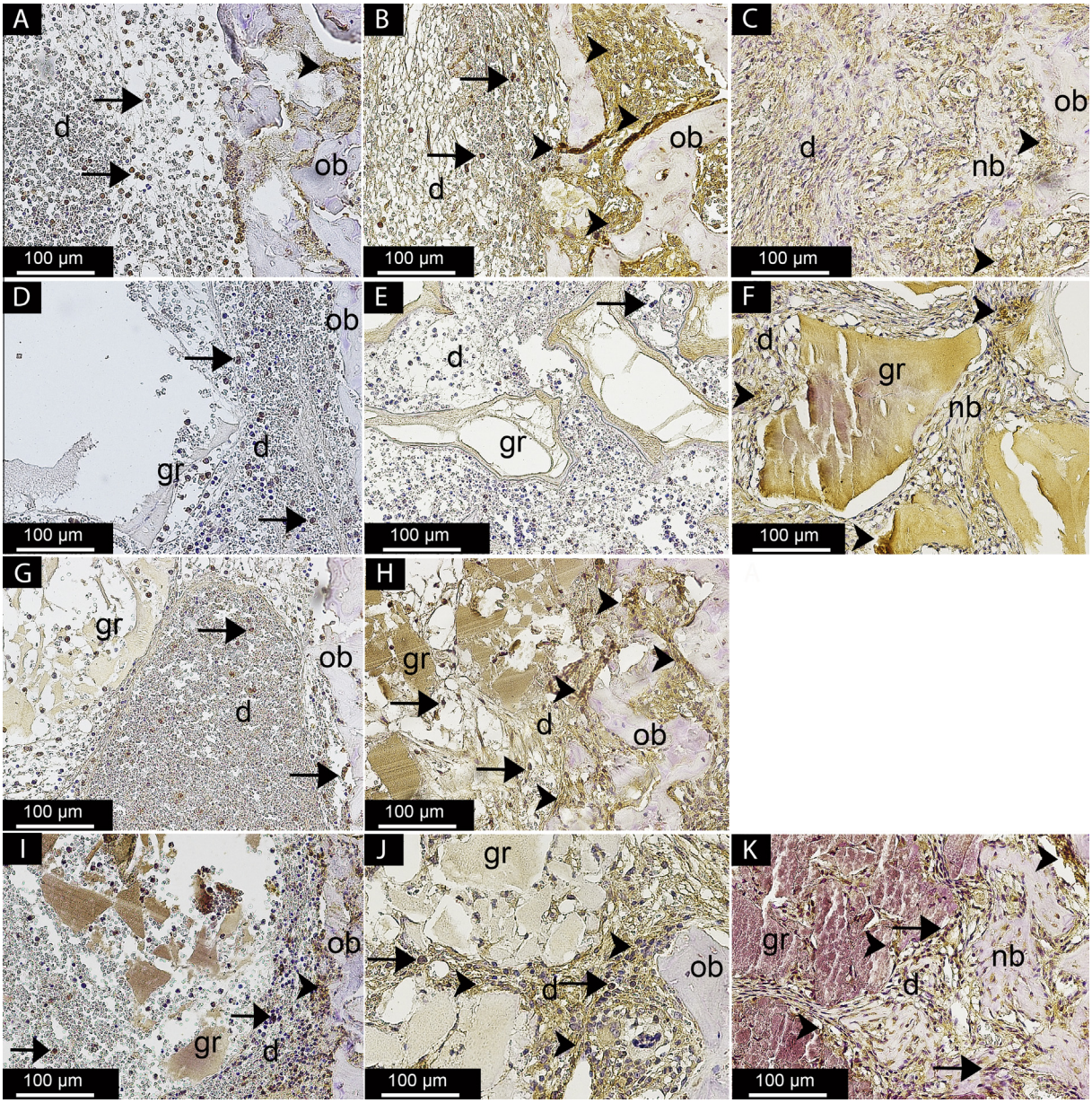

Fig. 5. Immunohistochemical analysis of periostin reactivity in the defects treated with membrane alone or membrane in combination with the different bone substitute materials. The survey micrographs show selected regions of the defects treated with the membrane alone (sham; A–C) or the membrane in combination with deproteinized bovine bone granules (DBB; D–F), hydroxyapatite granules (HA; G and H) or strontium-doped hydroxyapatite granules (SrHA; I–K). The analysis was performed at 12 h (A, D, G and I), 3 days (B, E, H and J) and 6 days (C, F and K) of implantation. The membrane with hydroxyapatite granules (HA) group at 6 days was excluded from this analysis due to technical limitations in obtaining proper paraffin-embedded sections. Black arrows = staining of osteoprogenitors; black arrowheads = diffuse staining of the intramembranous bone formation; ob = old bone; nb = new bone; d = defect; gr = granule.

Table 2
Immunohistochemical analysis of CD68-positive monocytes/macrophages in the defects treated by membrane alone (sham) or the membrane in combination with deproteinized bovine bone (DBB), hydroxyapatite (HA) or strontium-doped hydroxyapatite (SrHA) granules after 12 h, 3 days and 6 days of healing.

	Sham	DBB	HA	SrHA
12 h	+	+	+	+
3 days	++	+++	+++	+++
6 days	+++++	++++	ND	++++

Labeling: + = 1–100 cells/mm^2; ++ = 101–200 cells/mm^2; +++ = 201–400 cells/mm^2; ++++ = 401–800 cells/mm^2; +++++ > 800 cells/mm^2; ND = not done.

detected in the SrHA group as compared to the DBB-filled defects (Table 3). On the other hand, the CD68-positive osteoclasts were equally present in the sham and DBB groups, but there were considerably fewer in the SrHA group (Table 3). The MNGCs were seldom found in the sham defects.

3.3. Histomorphometry

The relative proportion of the newly formed (woven) bone was determined in the total defect area (Fig. 6), as well as in different regions of the defect (Fig. 6). Despite the generally low percentage of newly formed woven bone (ranging between 4% and 7.3% of the total defect area), the histomorphometric analysis revealed a significantly higher total bone area percentage in SrHA-treated defects (7.3 ± 0.6) compared with sham (3.7 ± 0.8).

The topological measurements at 6 d showed a higher proportion of new bone at the periphery (calculated per the peripheral

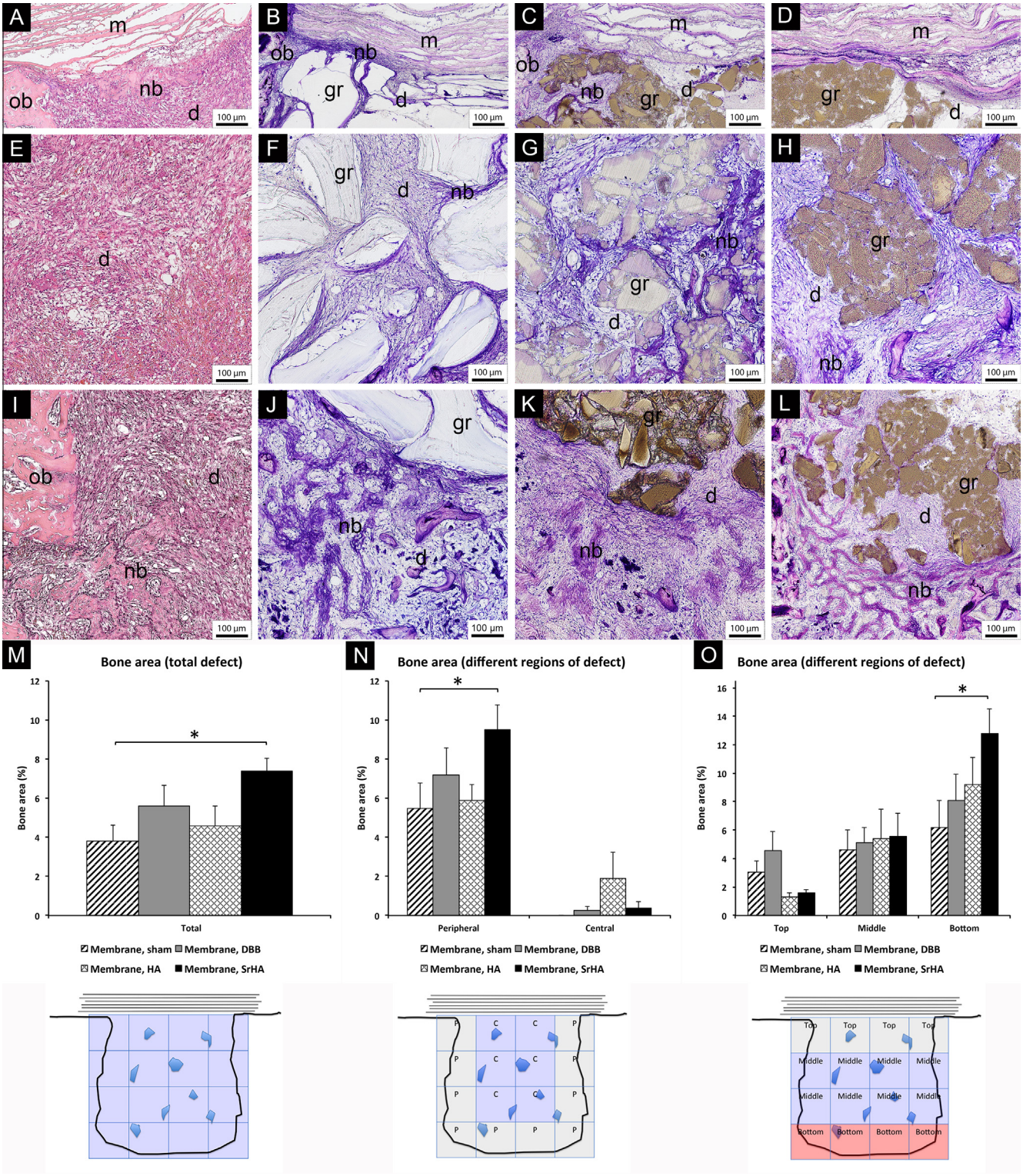

Fig. 6. Histology and histomorphometry of the defects treated with membrane alone or the membrane in combination with the different bone substitute materials. The light micrographs show the pattern of new bone (nb) formation in the top (A–D), middle (E–H) and bottom (I–L) regions of each defect (d) at 6 days of implantation. The defects were either empty (sham) (A, E and I) or filled with deproteinized bovine bone granules (DBB) (B, F and J), hydroxyapatite granules (HA) (C, G and K) or strontium-doped hydroxyapatite granules (SrHA) (D, H and L). Resorbable ECM membrane (m) was placed over each defect, above the granules (gr). The column graphs show the histomorphometric measurement of the new bone area in the entire defect (M), peripheral and central regions (N), as well as in the top, middle and bottom regions (O) of the defect. Statistically significant difference ($p < 0.05$) indicated by asterisk (*). The schematic diagrams show the defect and the area of measurements for histomorphometry. A software rectangular grid consisting of sixteen zones covered the entire area of the defect. C = central region; P = peripheral region. ob = old bone.

area) compared with the bone proportion found centrally in the respective central area. The SrHA demonstrated a significantly higher proportion of new bone in the peripheral region (9.5 ± 1.2%), compared with that found in the peripheral region of

Table 3
Immunohistochemical analysis of CD68-positive multinucleated cells in the defects treated by membrane alone (sham) or the membrane in combination with deproteinized bovine bone (DBB), hydroxyapatite (HA) or strontium-doped hydroxyapatite (SrHA) granules after 6 days of healing.

	Sham	DBB	HA	SrHA
Bone-related multinucleated cells (osteoclasts)	++	++	ND	+
Material-related multinucleated cells	–	++	ND	+++

Labeling: – = no cells; + = 1–5 cells/mm^2; ++ = 6–10 cells/mm^2; +++ ⩾ 10 cells/mm^2; ND = not done.

the sham (5.4 ± 1.3%). In all defects, newly formed woven bone was also seen at the top level, in close proximity to the lower surface of the membrane, but no significant differences were detected between the groups.

3.4. Histology and immunohistochemistry of the membrane compartment

At all time points, the membrane was localized above the defect separating the top granules or bone tissue from the overlying soft tissue (Fig. 3). At all time points (12 h, 3 d and 6 d; Figs. 7 and 8), mononuclear cells were evident inside the membrane, assuming access and migration through the peripheral borders, between the separated collagen layers of the membrane, rather than directly across the membrane. Immunostaining with CD68 (Fig. 7) and periostin (Fig. 8) revealed the existence of monocytes/macrophages and osteoprogenitors inside the membrane throughout the healing period. Both CD68 and periostin reactivity appeared to be restricted to well-defined mononuclear cells where neither multinuclear staining with CD68 nor diffuse staining with periostin was observed inside the membrane.

3.5. Gene expression in the different defects

Comparisons were made of gene expression in bone retrieved during the defect preparation (baseline; BL) and the tissue harvested from the sham and filled defects after 12 h, 3 d and 6 d. Selected examples of genes involved in the early events of bone healing, including cell recruitment and inflammation, bone formation and remodeling (Fig. 9), were analyzed.

3.5.1. Gene expression of cell recruitment and inflammation markers (Fig. 9)

3.5.1.1. Baseline and temporal changes in gene expression. Generally, the cell recruitment chemokines, MCP-1 and CXCR4, and the

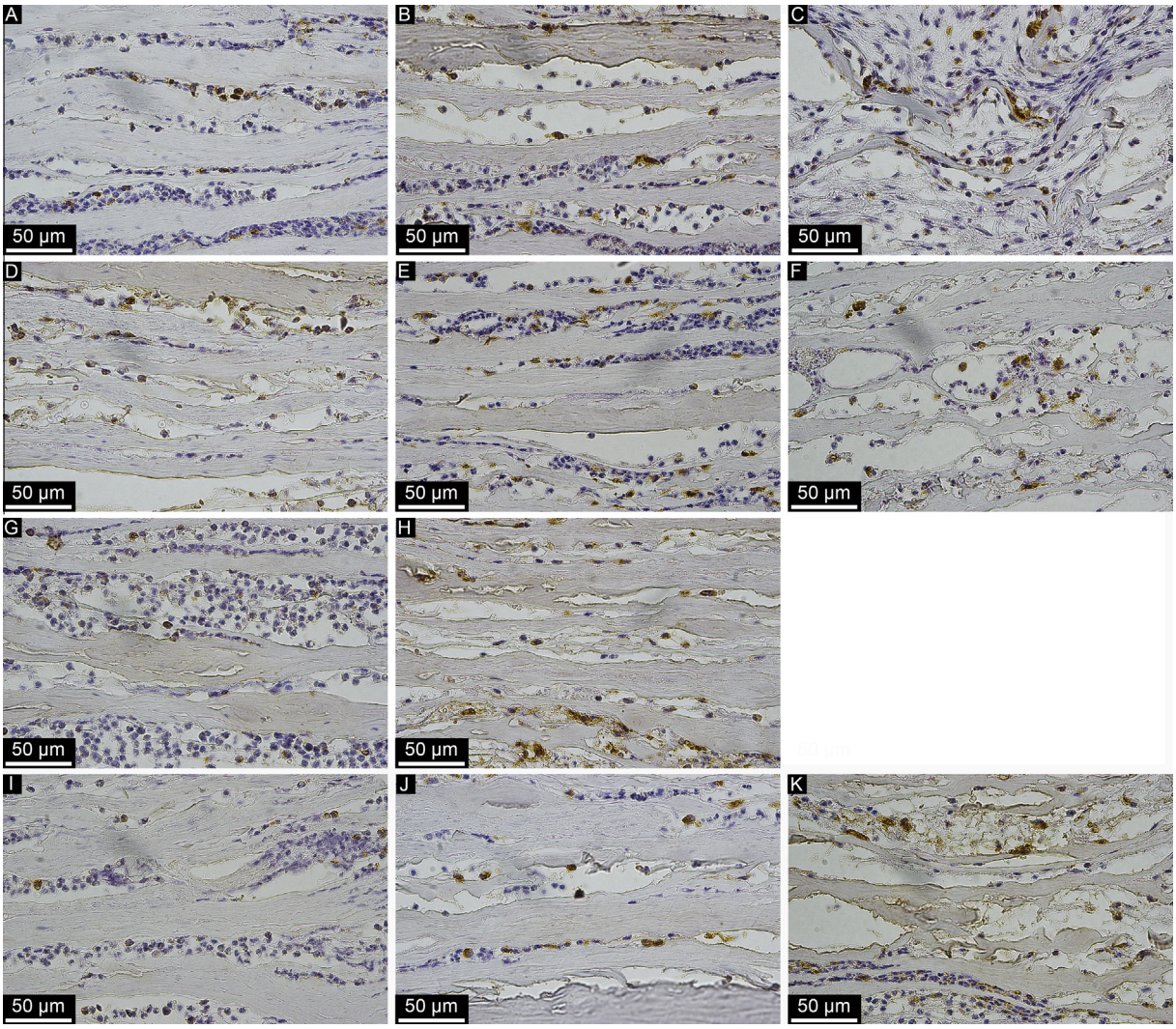

Fig. 7. Immunohistochemical analysis of CD68 reactivity in the membrane compartment above the defect. The defects were treated with membrane alone (sham; A–C) or the membrane in combination with deproteinized bovine bone (DBB; D–F), hydroxyapatite (HA; G and H) or strontium-doped hydroxyapatite (SrHA; I–K). The membrane with hydroxyapatite granules (HA) group at 6 days was excluded from this analysis due to technical limitations in obtaining proper paraffin-embedded sections. The micrographs show the CD68-positive cells in the membrane compartment at 12 h (A, D, G and I), 3 days (B, E, H and J) and 6 days (C, F and K) of defect healing.

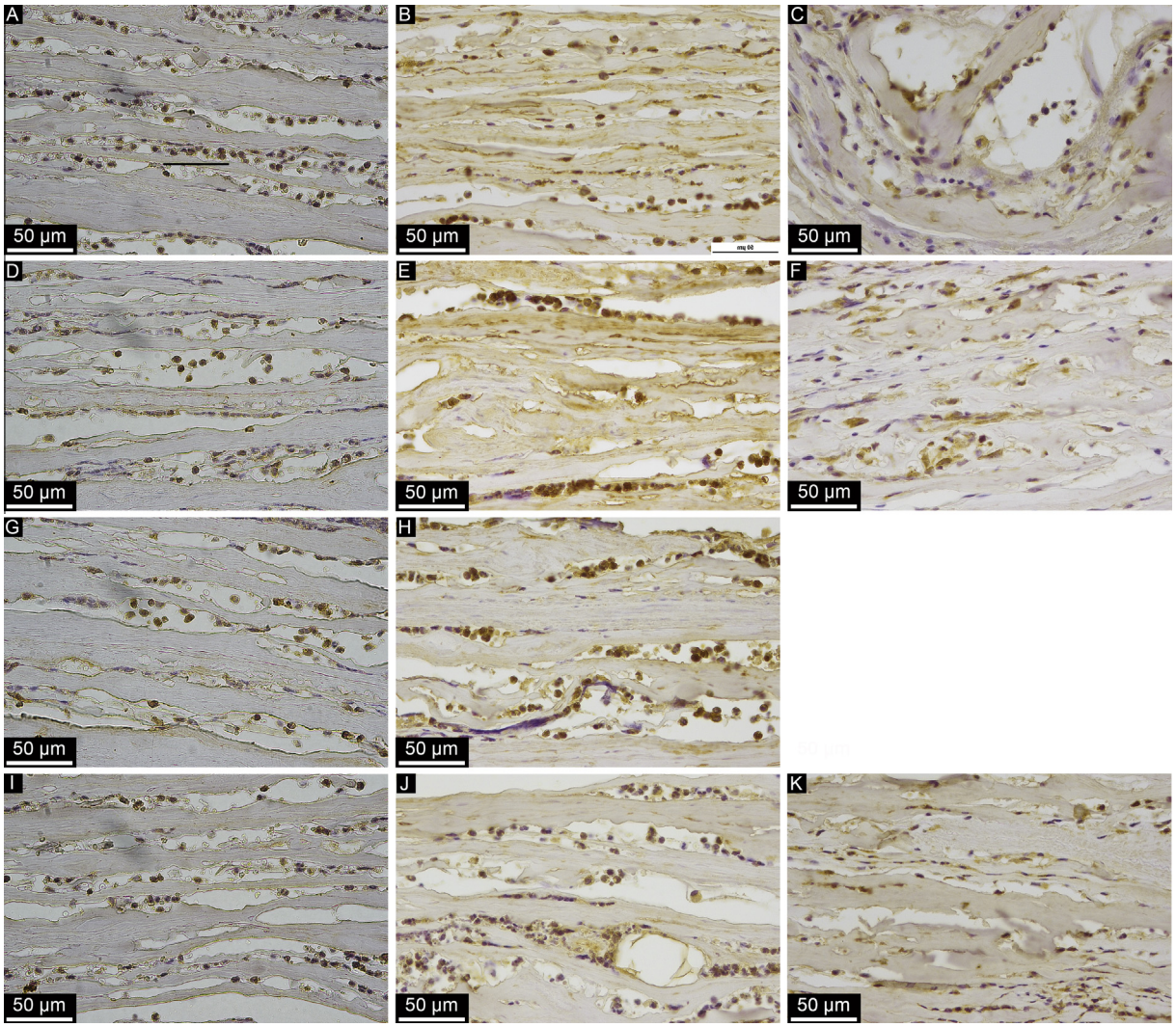

Fig. 8. Immunohistochemical analysis of periostin reactivity in the membrane compartment above the defect. The defects were treated with membrane alone (sham; A–C) or the membrane in combination with deproteinized bovine bone (DBB; D–F), hydroxyapatite (HA; G and H) or strontium-doped hydroxyapatite (SrHA; I–K). The membrane with hydroxyapatite granules (HA) group at 6 days was excluded from this analysis due to technical limitations in obtaining proper paraffin-embedded sections. The micrographs show the periostin-positive cells in the membrane compartment at 12 h (A, D, G and I), 3 days (B, E, H and J) and 6 days (C, F and K) of defect healing.

pro-inflammatory cytokine, IL-6, demonstrated significantly higher expression levels at all evaluated time points compared with the constitutive BL level, irrespective of the experimental groups (sham, DBB, HA or SrHA), and they were significantly reduced thereafter. In fact, the expression of IL-6 and MCP-1 in the BL was comparatively negligible. The peak expression of TNF-α, IL-6 and CXCR4 observed at 12 h revealed a significant reduction after 3 d, for all groups, but it was still significantly higher compared with the BL levels of these genes. A similar temporal trend was observed for MCP-1, but the temporal change from 12 h to 3 d was not statistically significant. From 3 d to 6 d, whereas CXCR4 and IL-6 maintained similar levels for all groups, TNF-α showed a further significant reduction to the lowest levels for all experimental groups. The MCP-1 was also significantly reduced from 3 d to 6 d for all groups except for the DBB group where no statistically significant change was observed.

3.5.1.2. Comparative gene expression between the groups. At 12 h, the SrHA significantly reduced the expression of IL-6, six-fold and two-fold, compared with the sham and HA, respectively. At the same time, DBB resulted in a two-fold significant upregulation of TNF-α when compared with the sham and HA. At 3 d, a 1.5-fold significantly lower expression of TNF-α was demonstrated in the SrHA and DBB groups when compared with the HA group. Moreover, the expression of CXCR4 was 1.6-fold significantly lower in the SrHA compared with the sham. At 6 d, no significant differences were detected for any of the pro-inflammatory genes or cell recruitment genes between the different groups.

3.5.2. Gene expression of bone formation and bone resorption markers (Fig. 9)

3.5.2.1. Baseline and temporal changes in gene expression. In contrast to the expression profile of the pro-inflammatory cytokines, the expression of all selected bone-formation and remodeling genes was characterized by high constitutive expression at BL that was significantly downregulated after 12 h for all groups (sham, DBB, HA and SrHA). After 3 d, whereas the expression levels of bone-formation genes (ALP and OC) remained significantly lower than the constitutive BL, the expression of remodeling genes (CR and RANKL) in all groups recovered to levels similar to the BL, except for the SrHA, where they remained significantly lower than the BL. After 6 d, the expression of bone-formation genes demonstrated an equal increase in all groups, reaching significantly higher levels than the BL. In parallel, the expression of the

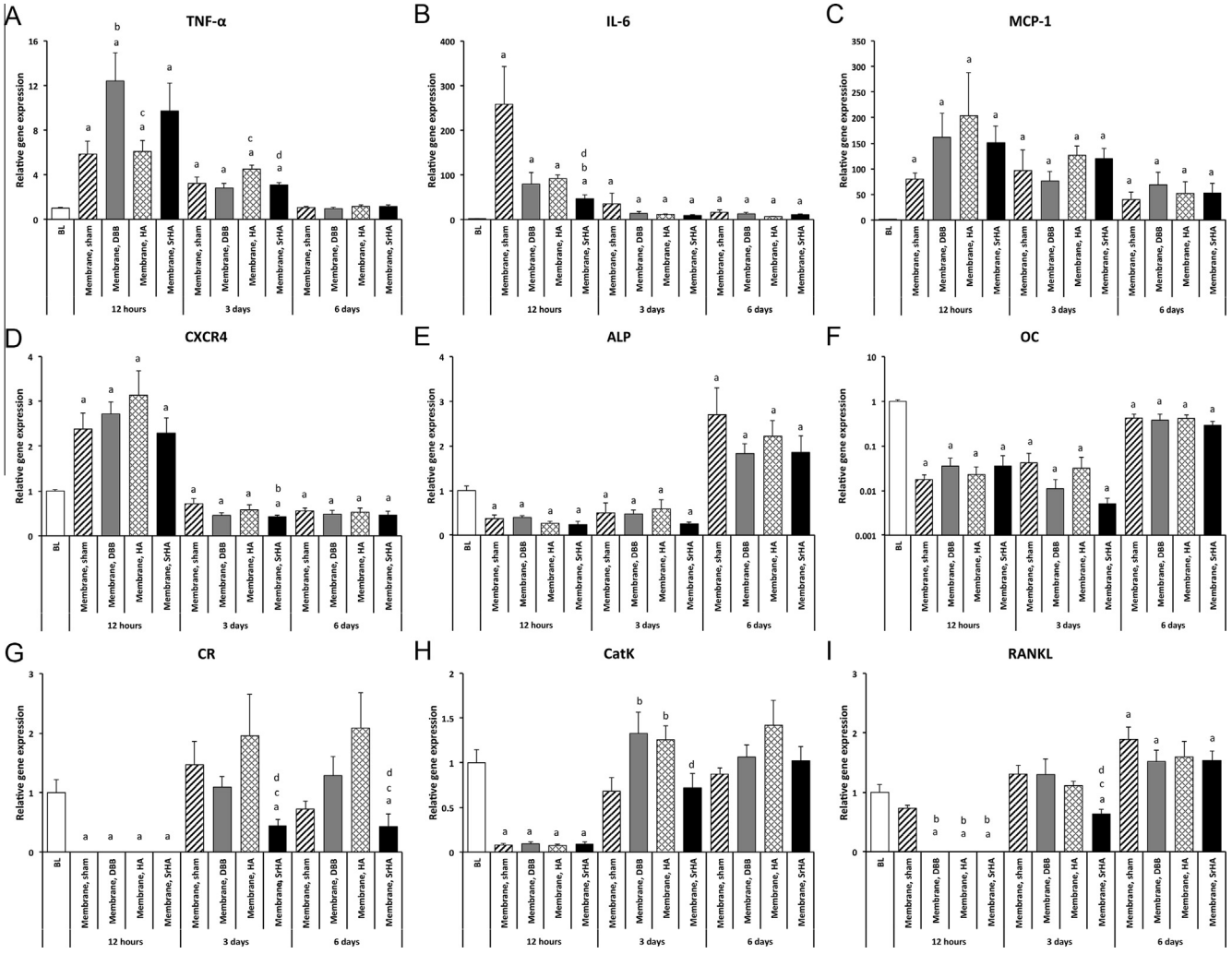

Fig. 9. Gene expression analysis of pro-inflammatory and cell recruitment, bone formation, bone resorption and remodeling markers in the bone defects after 12 h, 3 days and 6 days of healing. The defects were treated with membrane alone (sham) or the membrane in combination with deproteinized bovine bone (DBB), hydroxyapatite (HA) or strontium-doped hydroxyapatite (SrHA). Statistically significant differences ($p < 0.05$) are indicated by the small letters: a = significant difference from baseline (BL); b = significant difference from sham; c = significant difference from DBB; d = significant difference from HA. TNF-α = tumor necrosis factor; IL-6 = Interleukin 6; MCP-1 = monocyte chemoattractant protein-1; CXCR4 = chemokine receptor type 4; ALP = alkaline phosphatase; OC = osteocalcin; CR = calcitonin receptor; CatK = cathepsin K; RANKL = receptor activator of nuclear factor kappa-B ligand.

remodeling/coupling gene, RANKL, was also elevated to significantly exceed the BL level, with no major variation among the experimental groups. However, after 6 d, although the expression of CatK in all groups was maintained at a level similar to the BL, the osteoclastic surface marker, CR, was significantly lower than the BL. From 12 h to 3 d, a significant temporal increase was demonstrated for all osteoclastic genes (CR and CatK) in all groups. In parallel, from 12 h to 3 d, no major temporal change was observed in the expression of bone formation genes (ALP and OC) in any of the groups. From 3 d to 6 d, this relationship was reversed, whereby the expression of bone-formation genes (ALP and OC) significantly increased and the expression of osteoclastic genes (CR and CatK) did not change significantly for any group. The RANKL expression revealed a constant significant increase for all groups from 12 h to 3 d and from 3 d to 6 d.

3.5.2.2. Comparative gene expression between the groups. With regard to the expression of bone-formation markers (ALP and OC), no major significant differences were found between the different groups at any time point. At 12 h, the expression of RANKL was not detected in the defects with bone substitutes (DBB, HA and SrHA), while a significantly high level was demonstrated in the sham, unfilled defect. At this time point (12 h), the CR expression was also not detected in all groups, irrespective of whether they were filled or unfilled. No major differences were observed in the detected CatK expression levels between the groups at 12 h. At 3 d, the expression levels of CR and RANKL were 1.7- to two-fold and 2.5- to four-fold significantly lower in the SrHA compared with the other groups. The CatK expression was about 1.8- to two-fold lower in the SrHA and sham groups compared with the DBB and HA. At 6 d, the SrHA further demonstrated a 1.7- to five-fold lower expression of CR when compared with the other groups.

4. Discussion

The present study investigated the early molecular and structural events of bone healing in trabecular bone defects treated with naturally derived resorbable membrane with and without different bone substitutes. One major histological finding was the increased level of total bone formation, at 6 d, with SrHA granules. Interestingly, no significant added benefit of DBB and HA

substitutes on early bone development was detected in comparison to the membrane-covered, empty defect. Since all the defects were covered with a membrane, one possible explanation is that the membrane had created an optimal environment that promoted intra-membranous bone formation, even in the absence of introduced scaffolding materials. In support, a similar defect treated with only HA or SrCaP substitutes failed to generate new bone at early (6 d) but not late (28 d) time points, in the absence of a membrane [13]. Although both DBB and HA promote bone formation and defect restitution over time [14–16], the present results indicate that these materials are not optimal, osteoinductive materials, able to rapidly trigger osteogenesis and the filling of bone defects.

The mechanism for the enhanced bone formation induced by the presence of SrHA granules in the defect was explored. As judged by the results of the early (before 7 d) Ca, P and Sr ion-release patterns *in vitro*, the release of Sr was the main difference between SrHA and HA granules. One major explanation for the increase in the early amount of bone in association with the SrHA was the inhibition of osteoclastic differentiation and activity, as judged by the significant reduction in CR, the osteoclast receptor marker, and CatK, the osteoclast activity marker at 3 d and 6 d, compared with the HA. On the other hand, SrHA did not influence the anabolic activity (ALP and OC) in the defect differently from the other substitutes. This is in partial agreement with recent observations *in vitro,* [8]. The latter study confirmed a marked reduction in osteoclast number whereas no major change in the ALP activity or osteoblast number was observed when the cells were exposed to Sr ranelate in range of 0.1–1 mM, which is comparable to the Sr levels released by the present SrHA (0.2–1.5 mM; 3–7 d, respectively) *in vitro*. However, a major difference between the results of the two studies was the significant reduction of mineralization in the osteoblast culture [8]. Nevertheless, by virtue of the significant reduction in RANKL expression observed in the present study, it is possible that the major effect of Sr on osteoblasts was exerted through the de-coupling of the osteoblast–osteoclast cross-talk. This finding adds to previous observations that the presence of SrCaP materials significantly reduces the osteoclast gene expression but not the anabolic, osteoblast gene expression [13]. In the latter study, Sr did not affect RANKL expression at 6 d and 28 d, which indicates that the Sr effect on RANKL expression takes place during the very early time period (3 d).

Further supporting evidence of an interaction between Sr and osteoclasts was the observed reduction in the number of CD68 immunoreactive, multinuclear giant cells localized at resorption sites. Interestingly, SrHA was associated with an increase in the number of cells with a similar immune phenotype localized at the surface of the SrHA substitute. The interpretation of these findings is that the presence of Sr does not interfere with the formation of multinucleated giant cells. Multinucleated cells are either osteoclasts, which are differentiated from monocytes via specific intracellular signaling pathways [17], or "foreign-body giant cells", which are formed as a result of the fusion of multiple macrophages after frustrated phagocytosis [18,19]. In the present study, these cells were defined in the defect by immunostaining using CD68 antibody, which is a marker of all cell phenotypes of monocyte lineage, including macrophages, foreign-body giant cells and osteoclasts [19,20]. In fact, the multinucleated cells in the defects were detected in association with either the bone or the surface of the implanted granules. The bone-related multinuclear cells were assumed to be osteoclasts, based on their histological characteristics, proximity to newly formed bone and formation of resorption lacunae, although the osteoclastic phenotype of these cells was not further investigated in this study. At present, it is not possible to determine whether the multinucleated, CD68-positive cells localized on the surface of the substitute materials are osteoclasts. Previous studies of the phenotype of multinucleated giant cells around HA particles after implantation in rat bone defects have shown that these cells exhibit neither the morphologic nor the enzymatic and functional characteristics of the osteoclast [21]. Clinical, oral bone specimens have shown that synthetic HA is associated with more multinucleated giant cells compared with DBB [22]. There is evidence that "foreign-body giant cells" also produce vascular endothelial growth factor, which is an important molecule for angiogenesis during bone healing [22,23]. The significance of these material-related giant cells in relation to material degradation, repair and bone regeneration awaits clarification. In spite of this, their formation appears to be an integral process in the early period of bone regeneration with calcium phosphate substitutes. Taken together, the present and previous results show that synthetic SrHA is associated with lower osteoclast numbers and reduced osteoclast activity but a relatively large number of material-associated multinuclear giant cells.

The current results support pre-clinical and clinical data showing no difference in the osteogenic potential between the natural HA (DBB) and the synthetic HA [14–16]. Furthermore, the different materials revealed distinct patterns of bone distribution. In relation to the membrane-covered empty defect, a significantly larger and substantial amount of new bone formation had taken place in the peripheral and bottom parts of the defect in conjunction with the SrHA. Comparable data were reported in another recent study, where bone regeneration in association with HA was compared with strontium-doped calcium phosphate in a rat bone defect [13]. In the latter study, performed during a late time period (28 d), SrCaP induced a larger amount of bone in the periphery of the defects, whereas the HA promoted high bone regeneration centrally. One possible explanation for these different bone distribution patterns could be the release of strontium that was assumed to diffuse in the defect in a concentration gradient, with a low optimal level at the periphery and a high, perhaps even detrimental level at the center. *In vitro* studies show that the Sr effect on osteoblasts is multiphasic and dose dependent [24,25]. In the present study, the SrHA selected for the *in vivo* implantation was based on a cumulative Sr release *in vitro* comparable with optimal concentrations proposed in other *in vitro* studies [24,25].

In the present study, among the three SrHA preparations (SrHA005, SrHA025 and SrHA050) only the material with the highest level of Sr substitution in the HA (SrHA050) was used in the *in vivo* experiment. The main reason for this selection was that the *in vitro* release experiment showed that this group demonstrated the highest range of Sr ion (0.2–1.5 mM) while exhibiting a relatively stable low release of Ca and P, compared to the other two SrHA preparations. The selection of the SrHA preparation that released up to 1.5 mM Sr (SrHA050) is in accordance with previous *in vitro* studies showing that this range of Sr concentration is the most effective to induce anti-osteoclastic or both anti-osteoclastic and pro-osteoblastic responses [8,9,26]. On the other hand, Sr in low quantity in a magnesium-based alloy (2% Sr) induced new, fully mineralized trabecular bone, which remained in direct contact with the implanted material, as compared to similar alloy but with higher quantity of Sr (5%) [27]. Nevertheless, direct comparison between bone formation induced in the present study by the SrHA (with 50% Sr) and that induced by the Mg–Zr–Sr (with 2% Sr) [27] is hindered. This is due to major differences in the type of implanted material, animal model and observation periods.

Several *in vitro* studies have shown evidence for both pro-osteogenic (anabolic) and anti-resorptive (anti-catabolic) effects of Sr on osteoblasts [7,28,29] and osteoclasts [9], respectively. This has formed the prevailing hypothesis for using Sr as a dual acting agent in combination with bone substitutes [30,31] and implants [32]. In the present study, in order to explore the *in vivo* local effect of Sr incorporation in bone substitute material, the bone healing events were investigated in defects treated with a combination

of SrHA and GBR membrane. The present study, together with our previously published report using SrCaP without membrane [13], show that Sr-containing materials promote new bone formation in the defect. Firstly, after 6 d of healing, among different substitute materials, combining SrHA with the collagen membrane resulted in a higher level of woven bone formation compared to the membrane-alone treated defect. Secondly, at late time period, 28 d, the newly formed bone at the peripheral region of the defect was significantly higher in conjunction with the SrCaP compared to HA (both in normal and osteoporotic condition) [13]. These morphological observations are in agreement with recent *in vivo* data showing that incorporation of Sr with bone substitutes [33–35], collagen membranes [36], and titanium implants [32,37,38] enhance bone regeneration and osseointegration. Importantly, the present results extend the previous observation by demonstrating that the mechanism for this effect involves the reduction of osteoclast number and activity as well as the reduction of osteoblast–osteoclast coupling without affecting the osteoblast anabolic gene expression.

The early recruitment of cells was investigated in this study. The results show that, irrespective of the presence or absence of the substitute materials, both monocytes/macrophages and osteoprogenitors are recruited very rapidly to the site of bone healing. However, it was evident that the presence, and the type, of the substitute material affected the cell recruitment process. The first line of evidence in this study was the generally higher proportion of CD68-positive monocytes/macrophages in the defects filled with bone substitutes compared with unfilled defects. The second piece of evidence was that the SrHA significantly downregulated the expression of the major component of the cell recruitment axis, CXCR4. CXCR4 is a surface receptor expressed by various cells, including MSCs and osteoprogenitors [39,40], as well as osteoclast precursors [41]. In the present study, the SrHA-induced downregulation of CXCR4, in parallel with reduced osteoclast activity and number, suggests that at least part of the inhibitory effect of Sr on osteoclasts is exerted at the level of osteoclast precursor recruitment.

It has been shown that the inflammatory response of monocytes to biomaterials is affected by the material properties. For example, sintering the HA particles at high temperature induces changes in crystal shape and size, which has been shown to stimulate monocytes to produce more inflammatory cytokines [42]. It has also been suggested that needle- and irregular-shaped HA particles provoke a greater inflammatory response compared with spherical particles [42]. In the present study, the sintered synthetic HA granules (rough surface with irregular microparticles) induced higher TNF-α activity at 3 d, compared with the DBB granules, with a smooth surface and spherical microparticles. Furthermore, other *in vitro* studies have shown that the incorporation of Sr with CaP materials inhibits the production of TNF-α and IL-6 [43,44]. These findings are in agreement with the present *in vivo* observations: IL-6 and TNF-α expression levels were significantly reduced in defects with SrHA granules at 12 h and 3 d, respectively, compared with HA granules. Given the well-described role of pro-inflammatory cytokines in osteoclastogenesis, the modulation of TNF-α at this specific time point, 3 d, suggests an important role for this cytokine in the differentiation of osteoclast precursors. Further, the lower expression of TNF-α in the SrHA defect took place in parallel with the downregulation of RANKL, the main stimulatory factor in the formation of mature osteoclasts. This observation is in agreement with recent *in vitro* data showing the lower production of TNF-α and RANKL by macrophages and osteoblasts, respectively, when these cells were separately exposed to strontium-doped calcium polyphosphate particles in comparison with HA particles [45].

It has been suggested that the application of a membrane during guided bone regeneration serves as a passive barrier, preventing the migration of non-osteogenic cells to the defect site. In the present study, the membrane accumulated different cell phenotypes at different time periods of implantation. The histological observation of cells that had migrated into the membrane and the immunohistochemical identification of two major cell populations, monocytes/macrophages and osteoprogenitors, inside the membrane, at least partly contradict the prevailing view that the membrane acts as a physical barrier to cells. Their presence instead indicates that the membrane possesses properties that provide cues for cell migration, adhesion and differentiation. In fact, the present membrane, which consists of porcine, extracellular matrix (ECM)-derived material with 90% collagen [46] and smaller amounts of glycosaminoglycans [47], glycoproteins and growth factors [48], may have bioactive properties of importance for bone regeneration. Recent experimental studies have demonstrated that this membrane promotes bone regeneration in the defect by attracting cells which express and secrete growth factors inside the membrane [49]. These events in the membrane were found to be strongly correlated with bone regeneration in the defect.

In the present study, the Sprague Dawley rat was used as an experimental animal model. This model has been extensively used in bone tissue-engineering research, due to several advantages, including the low cost, small size and the well-known age and genetic background [50]. Moreover, there is considerable information about the molecular mechanisms of bone healing that have been obtained from fracture models in rodents [51–53]. Cellular components, cytokines and growth factors are generally well conserved between species and convey similar biological functions during inflammation and tissue regeneration. For instance, apart from proportional variations, monocyte subpopulations appear similar in humans, mice, and rats, especially when based on the expression of chemokine receptors, adhesion molecules, and differences in size and granularity [54,55]. On the other hand, there are some drawbacks for the rat animal model, which include the relatively high bone turnover and temporal variations in the rate of tissue healing and regeneration. In addition, there are anatomical disparities with larger animals and humans, such as the differences in bone macro- and micro-structure (e.g. the lack of Haversian system in the cortical bone [56]) as well as differences in the biomechanical properties). Taken together, it is worth to state that whereas the present study provided knowledge on fundamental biological processes of healing during bone augmentation and GBR, a direct extrapolation of the data to human conditions should be made with caution.

5. Conclusion

It is concluded that SrHA, but not DBB and HA, promotes early bone regeneration in defects covered with a resorbable collagenous membrane. The mechanism for the early SrHA-induced bone formation involves a reduced number of osteoclasts and the downregulation of the osteoclastic CatK and CR and the osteoblastic RANKL. These observations suggest that the effects of Sr *in vivo* are mediated by a reduction in catabolic and osteoblast–osteoclast coupling processes. The observation that monocytes/macrophages and osteoprogenitors are recruited into the membrane *per se* indicates that the membrane material may provide additional cues for substitute-driven bone regeneration.

Conflict of interest

None declared.

Acknowledgments

This study was supported by the BIOMATCELL VINN Excellence Center of Biomaterials and Cell Therapy, the Västra Götaland

Region, the Swedish Research Council (K2015-52X-09495-28-4), an LUA/ALF grant, the Stiftelsen Handlanden Hjalmar Svensson, the Vilhelm and Martina Lundgren Vetenskapsfond, the IngaBritt and Arne Lundberg Foundation and the Area of Advance Materials of Chalmers and GU Biomaterials within the Strategic Research Area initiative launched by the Swedish Government. The membrane used in the present study was kindly provided by Keystone Dental, Boston, USA.

Appendix A. Supplementary data

Supplementary data associated with this article can be found, in the online version, at http://dx.doi.org/10.1016/j.actbio.2015.10.005.

References

[1] F. Fontana, F. Santoro, C. Maiorana, G. Iezzi, A. Piattelli, M. Simion, Clinical and histologic evaluation of allogeneic bone matrix versus autogenous bone chips associated with titanium-reinforced e-PTFE membrane for vertical ridge augmentation: a prospective pilot study, Int. J. Oral Maxillofacial Implants 23 (2008) 1003–1012.
[2] C. Maiorana, D. Sigurta, A. Mirandola, G. Garlini, F. Santoro, Sinus elevation with alloplasts or xenogenic materials and implants: an up-to-4-year clinical and radiologic follow-up, Int. J. Oral Maxillofacial Implants 21 (2006) 426–432.
[3] D. Carmagnola, P. Adriaens, T. Berglundh, Healing of human extraction sockets filled with Bio-Oss, Clin. Oral Implants Res. 14 (2003) 137–143.
[4] A. Stavropoulos, L. Kostopoulos, N. Mardas, J.R. Nyengaard, T. Karring, Deproteinized bovine bone used as an adjunct to guided bone augmentation: an experimental study in the rat, Clin. Implant Dentistry Related Res. 3 (2001) 156–165.
[5] E. Boanini, M. Gazzano, A. Bigi, Ionic substitutions in calcium phosphates synthesized at low temperature, Acta Biomater. 6 (2010) 1882–1894.
[6] S. Peng, X.S. Liu, T. Wang, Z. Li, G. Zhou, K.D. Luk, et al., In vivo anabolic effect of strontium on trabecular bone was associated with increased osteoblastogenesis of bone marrow stromal cells, J. Orthopaedic Res. Official Publication Orthopaedic Res. Soc. 28 (2010) 1208–1214.
[7] F. Yang, D. Yang, J. Tu, Q. Zheng, L. Cai, L. Wang, Strontium enhances osteogenic differentiation of mesenchymal stem cells and in vivo bone formation by activating Wnt/catenin signaling, Stem Cells (Dayton, Ohio) 29 (2011) 981–991.
[8] D.P. Wornham, M.O. Hajjawi, I.R. Orriss, T.R. Arnett, Strontium potently inhibits mineralisation in bone-forming primary rat osteoblast cultures and reduces numbers of osteoclasts in mouse marrow cultures, Osteoporos. Int. 25 (2014) 2477–2484.
[9] R. Baron, Y. Tsouderos, In vitro effects of S12911-2 on osteoclast function and bone marrow macrophage differentiation, Eur. J. Pharmacol. 450 (2002) 11–17.
[10] E. Bonnelye, A. Chabadel, F. Saltel, P. Jurdic, Dual effect of strontium ranelate: stimulation of osteoblast differentiation and inhibition of osteoclast formation and resorption in vitro, Bone 42 (2008) 129–138.
[11] I. Elgali, K. Igawa, A. Palmquist, M. Lenneras, W. Xia, S. Choi, et al., Molecular and structural patterns of bone regeneration in surgically created defects containing bone substitutes, Biomaterials 35 (2014) 3229–3242.
[12] T.G. Kashima, T. Nishiyama, K. Shimazu, M. Shimazaki, I. Kii, A.E. Grigoriadis, et al., Periostin, a novel marker of intramembranous ossification, is expressed in fibrous dysplasia and in c-Fos-overexpressing bone lesions, Hum. Pathol. 40 (2009) 226–237.
[13] C. Cardemil, I. Elgali, W. Xia, L. Emanuelsson, B. Norlindh, O. Omar, et al., Strontium-doped calcium phosphate and hydroxyapatite granules promote different inflammatory and bone remodelling responses in normal and ovariectomised rats, PloS One 8 (2013) e84932.
[14] G.A. Gholami, B. Najafi, F. Mashhadiabbas, W. Goetz, S. Najafi, Clinical, histologic and histomorphometric evaluation of socket preservation using a synthetic nanocrystalline hydroxyapatite in comparison with a bovine xenograft: a randomized clinical trial, Clin. Oral Implants Res. 23 (2012) 1198–1204.
[15] S.S. Kim, B.S. Kim, Comparison of osteogenic potential between apatite-coated poly(lactide-co-glycolide)/hydroxyapatite particulates and Bio-Oss, Dent. Mater. J. 27 (2008) 368–375.
[16] P. Sponer, M. Strnadova, K. Urban, In vivo behaviour of low-temperature calcium-deficient hydroxyapatite: comparison with deproteinised bovine bone, Int. Orthopaedics 35 (2011) 1553–1560.
[17] M. Asagiri, H. Takayanagi, The molecular understanding of osteoclast differentiation, Bone 40 (2007) 251–264.
[18] J.M. Anderson, Biological responses to materials, Annu. Rev. Mater. Res. 31 (2001) 81–110.
[19] A.K. McNally, J.M. Anderson, Foreign body-type multinucleated giant cells induced by interleukin-4 express select lymphocyte co-stimulatory molecules and are phenotypically distinct from osteoclasts and dendritic cells, Exp. Mol. Pathol. 91 (2011) 673–681.
[20] L. Chun, J. Yoon, Y. Song, P. Huie, D. Regula, S. Goodman, The characterization of macrophages and osteoclasts in tissues harvested from revised total hip prostheses, J. Biomed. Mater. Res. 48 (1999) 899–903.
[21] J.M. Dersot, M.L. Colombier, J. Lafont, B. Baroukh, D. Septier, J.L. Saffar, Multinucleated giant cells elicited around hydroxyapatite particles implanted in craniotomy defects are not osteoclasts, Anatomical Record 242 (1995) 166–176.
[22] S. Ghanaati, M. Barbeck, J. Lorenz, S. Stuebinger, O. Seitz, C. Landes, et al., Synthetic bone substitute material comparable with xenogeneic material for bone tissue regeneration in oral cancer patients: first and preliminary histological, histomorphometrical and clinical results, Ann. Maxillofacial Surg. 3 (2013) 126–138.
[23] S. Ghanaati, M. Barbeck, C. Orth, I. Willershausen, B.W. Thimm, C. Hoffmann, et al., Influence of beta-tricalcium phosphate granule size and morphology on tissue reaction in vivo, Acta Biomater. 6 (2010) 4476–4487.
[24] J. Braux, F. Velard, C. Guillaume, S. Bouthors, E. Jallot, J.M. Nedelec, et al., A new insight into the dissociating effect of strontium on bone resorption and formation, Acta Biomater. 7 (2011) 2593–2603.
[25] M. Schumacher, A. Lode, A. Helth, M. Gelinsky, A novel strontium(II)-modified calcium phosphate bone cement stimulates human-bone-marrow-derived mesenchymal stem cell proliferation and osteogenic differentiation in vitro, Acta Biomater. 9 (2013) 9547–9557.
[26] T.C. Brennan, M.S. Rybchyn, W. Green, S. Atwa, A.D. Conigrave, R.S. Mason, Osteoblasts play key roles in the mechanisms of action of strontium ranelate, Br. J. Pharmacol. 157 (2009) 1291–1300.
[27] Y. Li, C. Wen, D. Mushahary, R. Sravanthi, N. Harishankar, G. Pande, et al., Mg–Zr–Sr alloys as biodegradable implant materials, Acta Biomater. 8 (2012) 3177–3188.
[28] W.-T. Su, W.-L. Chou, C.-M. Chou, Osteoblastic differentiation of stem cells from human exfoliated deciduous teeth induced by thermosensitive hydrogels with strontium phosphate, Mater. Sci. Eng. C 52 (2015) 46–53.
[29] S. Peng, G. Zhou, K.D. Luk, K.M. Cheung, Z. Li, W.M. Lam, et al., Strontium promotes osteogenic differentiation of mesenchymal stem cells through the Ras/MAPK signaling pathway, Cellular physiology and biochemistry: international journal of experimental cellular physiology, biochemistry, and pharmacology 23 (2009) 165–174.
[30] S. Kumar, K. Chatterjee, Strontium eluting graphene hybrid nanoparticles augment osteogenesis in a 3D tissue scaffold, Nanoscale 7 (2015) 2023–2033.
[31] M.E. Santocildes-Romero, A. Crawford, P.V. Hatton, R.L. Goodchild, I.M. Reaney, C.A. Miller, The osteogenic response of mesenchymal stromal cells to strontium-substituted bioactive glasses, J. Tissue Eng. Regenerative Med. 9 (2015) 619–631.
[32] Y. Liang, H. Li, J. Xu, X. Li, X. Li, Y. Yan, et al., Strontium coating by electrochemical deposition improves implant osseointegration in osteopenic models, Exp. Ther. Med. 9 (2015) 172–176.
[33] Y. Li, X. Shui, L. Zhang, J. Hu, Cancellous bone healing around strontium-doped hydroxyapatite in osteoporotic rats previously treated with zoledronic acid, J. Biomed. Mater. Res. B Appl. Biomater. (2015).
[34] Y. Zhang, X. Cui, S. Zhao, H. Wang, M.N. Rahaman, Z. Liu, et al., Evaluation of injectable strontium-containing borate bioactive glass cement with enhanced osteogenic capacity in a critical-sized rabbit femoral condyle defect model, ACS Appl. Mater. Interfaces 7 (2015) 2393–2403.
[35] Y. Zhang, L. Wei, C. Wu, R.J. Miron, Periodontal regeneration using strontium-loaded mesoporous bioactive glass scaffolds in osteoporotic rats, PLoS One 9 (2014) e104527.
[36] S. Kitayama, L.O. Wong, L. Ma, J. Hao, S. Kasugai, N.P. Lang, et al., Regeneration of rabbit calvarial defects using biphasic calcium phosphate and a strontium hydroxyapatite-containing collagen membrane, Clin. Oral Implants Res. (2015).
[37] J. Zhang, L. Liu, S. Zhao, H. Wang, G. Yang, Characterization and in vivo evaluation of trace element-loaded implant surfaces in ovariectomized rats, Int. J. Oral Maxillofacial Implants (2015).
[38] S.D. Newman, N. Lotfibakhshaiesh, M. O'Donnell, X.F. Walboomers, N. Horwood, J.A. Jansen, et al., Enhanced osseous implant fixation with strontium-substituted bioactive glass coating, Tissue Eng. A 20 (2014) 1850–1857.
[39] M. Kucia, J. Ratajczak, R. Reca, A. Janowska-Wieczorek, M.Z. Ratajczak, Tissue-specific muscle, neural and liver stem/progenitor cells reside in the bone marrow, respond to an SDF-1 gradient and are mobilized into peripheral blood during stress and tissue injury, Blood Cells Mol. Diseases 32 (2004) 52–57.
[40] W. Zhu, G. Liang, Z. Huang, S.B. Doty, A.L. Boskey, Conditional inactivation of the CXCR4 receptor in osteoprecursors reduces postnatal bone formation due to impaired osteoblast development, J. Biol. Chem. 286 (2011) 26794–26805.
[41] L.M. Wright, W. Maloney, X. Yu, L. Kindle, P. Collin-Osdoby, P. Osdoby, Stromal cell-derived factor-1 binding to its chemokine receptor CXCR4 on precursor cells promotes the chemotactic recruitment, development and survival of human osteoclasts, Bone 36 (2005) 840–853.
[42] A. Grandjean-Laquerriere, P. Laquerriere, D. Laurent-Maquin, M. Guenounou, T.M. Phillips, The effect of the physical characteristics of hydroxyapatite particles on human monocytes IL-18 production in vitro, Biomaterials 25 (2004) 5921–5927.
[43] E. Buache, F. Velard, E. Bauden, C. Guillaume, E. Jallot, J.M. Nedelec, et al., Effect of strontium-substituted biphasic calcium phosphate on inflammatory mediators production by human monocytes, Acta Biomater. 8 (2012) 3113–3119.
[44] X. Liu, S. Zhu, J. Cui, H. Shao, W. Zhang, H. Yang, et al., Strontium ranelate inhibits titanium-particle-induced osteolysis by restraining inflammatory osteoclastogenesis in vivo, Acta Biomater. 10 (2014) 4912–4918.

[45] C. Huang, L. Li, X. Yu, Z. Gu, X. Zhang, The inhibitory effect of strontium-doped calcium polyphosphate particles on cytokines from macrophages and osteoblasts leading to aseptic loosening in vitro, Biomed. Mater. (Bristol, England) 9 (2014) 025010.
[46] S.F. Badylak, R. Record, K. Lindberg, J. Hodde, K. Park, Small intestinal submucosa: a substrate for in vitro cell growth, J. Biomater. Sci. Polym. Ed. 9 (1998) 863–878.
[47] J.P. Hodde, S.F. Badylak, A.O. Brightman, S.L. Voytik-Harbin, Glycosaminoglycan content of small intestinal submucosa: a bioscaffold for tissue replacement, Tissue Eng. 2 (1996) 209–217.
[48] J. Hodde, A. Janis, D. Ernst, D. Zopf, D. Sherman, C. Johnson, Effects of sterilization on an extracellular matrix scaffold: part I. Composition and matrix architecture, J. Mater. Sci. Mater. Med. 18 (2007) 537–543.
[49] A. Turri, I. Elgali, F. Vazirisani, A. Johansson, L. Emanuelsson, C. Dahlin, et al., Guided bone regeneration is promoted by the molecular events in the membrane compartment. Submitted for Publication.
[50] P.F. O'Loughlin, S. Morr, L. Bogunovic, A.D. Kim, B. Park, J.M. Lane, Selection and development of preclinical models in fracture-healing research, J. Bone Joint Surg. 90 (2008) 79–84.
[51] J. Aurégan, R. Coyle, J. Danoff, R. Burky, Y. Akelina, M. Rosenwasser, The rat model of femur fracture for bone and mineral research an improved description of expected comminution, quantity of soft callus and incidence of complications, Bone Joint Res. 2 (2013) 149–154.
[52] T. Histing, P. Garcia, J. Holstein, M. Klein, R. Matthys, R. Nuetzi, et al., Small animal bone healing models: standards, tips, and pitfalls results of a consensus meeting, Bone 49 (2011) 591–599.
[53] V. Bentolila, T. Boyce, D. Fyhrie, R. Drumb, T. Skerry, M. Schaffler, Intracortical remodeling in adult rat long bones after fatigue loading, Bone 23 (1998) 275–281.
[54] D. Strauss-Ayali, S.M. Conrad, D.M. Mosser, Monocyte subpopulations and their differentiation patterns during infection, J. Leukocyte Biol. 82 (2007) 244–252.
[55] L. Ziegler-Heitbrock, Monocyte subsets in man and other species, Cell Immunol. 289 (2014) 135–139.
[56] P. Gomes, M. Fernandes, Rodent models in bone-related research: the relevance of calvarial defects in the assessment of bone regeneration strategies, Lab. Anim. 45 (2011) 14–24.